Internal Tides in the Strait of Gibraltar

EUGENE G. MOROZOV

Shirshov Institute of Oceanology, Russian Academy of Sciences, Moscow, Russia

KARSTEN TRULSEN* AND MANUEL G. VELARDE+

Instituto Pluridisciplinar, Madrid, Spain

VASILY I. VLASENKO

Marine Hydrophysical Institute, National Academy of Sciences, Sebastopol, Ukraine

(Manuscript received 15 April 2001, in final form 29 April 2002)

ABSTRACT

Analysis of moored current measurements in the Strait of Gibraltar is provided here. The vertical internal displacements (double amplitudes) with a semidiurnal frequency are extremely large and sometimes exceed 200 m. It is found that these displacements are associated with forced tidal internal waves over Camarinal Sill, which crosses the strait. The separation of tidal components showed that the amplitude of internal tide with M_2 frequency is 69 m, while the amplitudes of other components of the internal tide (S_2, K_1, O_1) are 3–5 times smaller. The amplitudes of the waves decrease with the distance from the sill and, at a distance of 50 km from the sill, the amplitudes are 3 times smaller than over the sill. The energy of internal tides is transferred to internal bore and turbulent mixing. The wavelength of the internal tide was estimated on the basis of moored measurements. The wavelength of the east-propagated wave is 90 km, while the west-propagated wave is 60 km. Numerical modeling demonstrates that the lower current in the strait directed from the Mediterranean Sea to the ocean, which occupies the major part of the water column, has a significant influence on internal tides. The effect of internal waves propagating in a hydraulic flow leads to the formation of an internal bore, followed by a wave packet of shorter internal waves. The shear formed by two opposite currents intensifies the bore and short-period internal waves in the eastern part of the strait in the upper layer.

1. Introduction

The Strait of Gibraltar is characterized by a two-layer system of opposite flows resulting from the difference in water density (salinity and temperature) between the Atlantic Ocean and the Mediterranean Sea. A strong surface current of relatively fresher water from the ocean compensates for intensive evaporation in the Mediterranean. A deep-water current of more saline Mediterranean Water flows into the ocean. A barotropic tidal wave is imposed on this system with velocities in the range 70–80 cm s^{-1}, about the same order of magnitude as the mean velocities of the currents between the ocean and the sea, and thus an unsteady flow is formed. The tide generates an internal wave when the tidal currents flow over uneven topography in the Strait, especially over Camarinal Sill. Lacombe and Richez (1982) gave a review of historical data about the currents and hydrographic regime in the strait and observations of an internal bore.

The flow regime and internal waves in the Strait of Gibraltar have been intensively studied during the past decades. The study by Bryden et al. (1994) provided evidence that the exchange across the Strait of Gibraltar is due in nearly equal parts to the mean currents and to tidal fluctuations. Their estimate for the Mediterranean Water outflow is equal to -0.68 Sv (Sv $\equiv 10^6$ m^3 s^{-1}), while the flow of Atlantic waters is 0.72 Sv, which equals to the sum of the outflow and net evaporation that is approximately 52 cm of the sea level per year. This estimate based on the direct measurements of currents is lower, by almost a factor of 2, than the previously reported values (Hopkins 1978; Lacombe and Richez 1982).

Bray et al. (1995) consider that a two-layer approach is insufficient to account for the flow regime in the strait.

* Current affiliation: SINTEF Applied Mathematics, Oslo, Norway.
+ Additional affiliation: International Center for Mechanical Sciences (CISM), Udine, Italy.

Corresponding author address: Dr. Manuel G. Velarde, Instituto Pluridisciplinar, Universidad Complutense de Madrid, 1 Paseo Juan XXIII, 28040 Madrid, Spain.
E-mail: velarde@fluidos.pluri.ucm.es

They extended the traditional Knudsen model of exchange to three layers, assuming that the interface is a transport-carrying third layer with uniform vertical shear. They found that as much as half of the inflowing and outflowing transports occurs in the interface layer, while vertical exchange between layers is comparable to about half of the horizontal exchange. An essential role in the vertical exchange is played by internal waves. The finite thickness of the halocline is important both kinematically and dynamically. The transition between Atlantic and Mediterranean waters in the strait is clearly marked by the halocline. It does not typically coincide with the thermocline, as there is a strong seasonal thermocline within the surface Atlantic water for much of the year. As a result, density profiles may have two pycnoclines, one for the seasonal thermocline and another for the halocline. Bray et al. (1990) analyzed the internal tide on the basis of CTD survey, yo-yo casts, and moorings. They give the analysis of semidiurnal fluctuations of the interface based on 1) hourly maps of hydrographic fields, 2) empirical orthogonal function decomposition of the hourly maps, and 3) harmonic analysis of the interface fluctuations inferred from moored measurements. Horizontal transport within the layer changes dramatically with distance along the strait, implying substantial vertical exchange between the interface and the upper and lower layers. At the eastern end of the strait, roughly half of the transport into the Mediterranean is found in the interface layer, while at the west end an equivalent outflowing transport occurs in the interface layer. On the other hand, little transport within the interface layer is observed near Camarinal Sill. The interface is deeper, thicker, fresher, and cooler at the west end of the strait than in the Tarifa Narrows, where a minimum in thickness and a maximum in salinity gradient are found. The thickness and depth of the pycnocline may be greatly influenced by internal waves. La Violette and Amone (1988) found that the turbulence resulting from an internal jump over Camarinal Sill might be the major mixing mechanism between the inflowing and outflowing water masses.

The exchange flow in the strait was also extensively studied by Armi and Farmer (1988). They showed that the flow regime periodically changes from subcritical to supercritical depending on the phase of the tidal wave. This process is hydraulically controlled at least over Camarinal and Spartel Sills, and perhaps also in the Tarifa Narrows, while the Tangiers Basin and the basin east of the Tarifa Narrows play the role of reservoirs accumulating the transported water. If the speed of the current exceeds that of the fastest gravity waves, a ''critical flow'' is reached so that the waves cannot propagate upstream. In this case the motion in the critical regime region is cut off from the influence of the downstream areas because the waves cannot propagate upstream. Thus, this flow is hydraulically controlled. Armi and Farmer (1988) also noted a very important feature in the strait. A rapid deepening of the interface in-phase with the tide occurs each 12 h west of Camarinal Sill. It is followed by the sudden eastward acceleration of the upper-layer flow, which yields an internal bore or density and velocity front. As described by Lacombe and Richez (1982), the interface deepens more than 200 m in 1 h, while at the same time the surface currents increase by 1 m s^{-1}. In the Tarifa Narrows this coincides with the passage of a series of surface ''slicks'' propagating eastward with a speed of about 1.5 m s^{-1}. This phenomenon is known as the tidal bore, usually observed when a tidal wave propagates upstream in a river. In the eastern part of the Strait of Gibraltar, an easterly propagating internal tidal wave propagates in the water column, the major part of which is occupied by the mean oppositely directed outflow current from the Mediterranean. A train of high frequency internal waves is observed on the trailing edge of the internal tide. Pettigrew and Needell (1989) reported about the records of these wave trains, measured by bottom based ADCP. The leading edge of the recorded internal tide is flatter than the trailing edge. These wave packets withdraw energy from the internal tide.

Measurements by Bockel (1962) indicate that the vertical displacements induced by tidal internal waves in the strait may exceed 200 m. This paper is a report of little known field measurements, became extremely popular in Russia after being cited in the book *Variability of the World Ocean* (Monin et al. 1974). Not many measurements demonstrate these extreme amplitudes of internal waves, except for Boyce (1975) whose measurements were made exactly over the sill. Other authors have also emphasized that the amplitudes are large but do not exceed 100 m (Watson 1994). Recent moored measurements at the eastern section of the strait (Lafuente et al. 2000) indicate that the internal tide there is not as strong as at Camarinall Sill. It is a helpful coincidence that the measurements of Bockel (1962) and the moorings of the 1985–86 Gibraltar experiment (Kinder and Bryden 1987) were located in the same place over Camarinal Sill.

Many papers report observations of various types of data about wave packets propagating in the eastern part of the strait. The surface slicks formed by these waves are clearly seen on a photograph from space (DAAC/NASA 1996, p. 89). These packets are observed almost each tidal cycle. Watson and Robinson (1990) gives a summary of the properties of these waves reported in about 20 papers. The period of the waves is around 10–20 min, the packet width is about 10–15 km, its duration is several hours, and the wavelength in the packet varies from 0.5 to 2.5 km. The peak-to-peak amplitudes may reach 50–60 m. Thermistor chains used by Ziegenbein (1969, 1970) allowed him to make records of the undular bore and associated solitary waves. The largest of these waves break and cause mixing, as observed by Wesson and Gregg (1988, 1994) with the microstructure profilers.

The measurements of Ziegenbein (1969) demonstrate

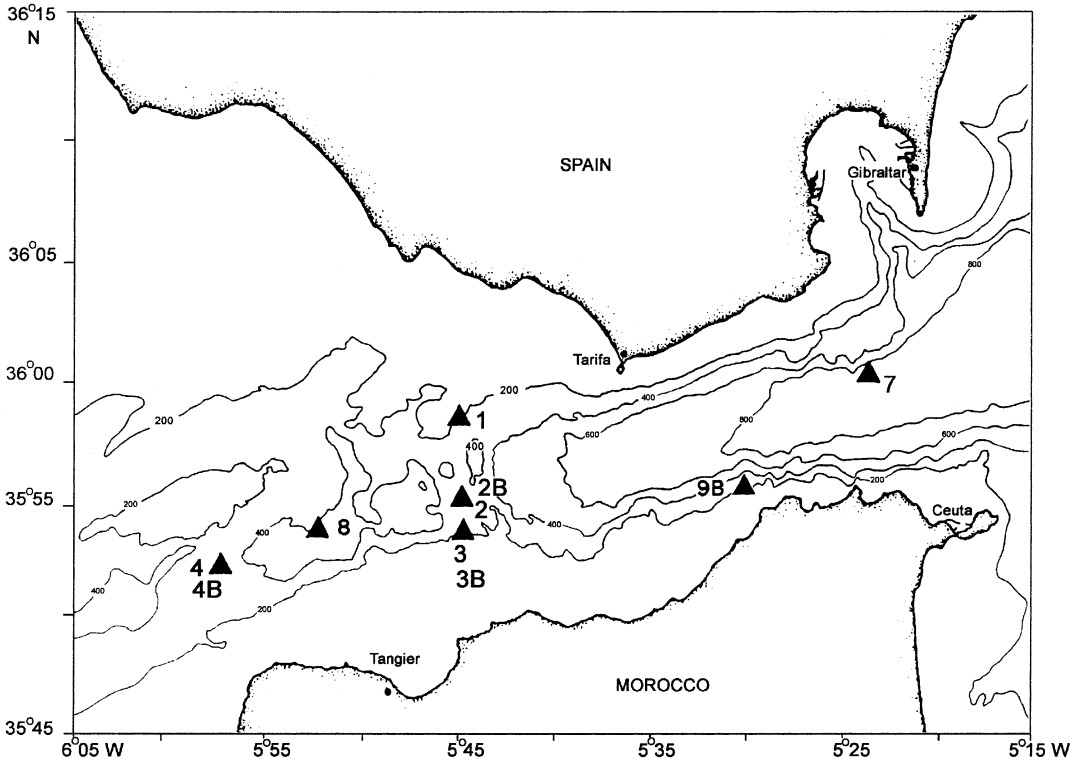

FIG. 1. Locations of moorings during the Gibraltar experiment in 1985–86. The moorings without suffix B were set for the period from Oct 1985 to May 1986. The moorings with suffix B were set from May 1986 to Oct 1986.

that intermittent trains of short-period internal waves associated with the tidal waves are found east of the sill, which indicates that tidal internal waves lose their energy to waves of shorter periods. Enhanced mixing, studied by Wesson and Gregg (1994) is also evidence of the high level of energy dissipation in the strait. A model proposed by Brunt et al. (1996) describes the decay of internal tides into trains of internal solitary waves on the basis of two-layer approach.

Armi and Farmer (1988) also indicated the existence of a weaker westward-propagating bore. It is released from the sill, near the low-water phase at the end of the inflowing (eastward) tide. This wave is less apparent than the eastward-propagating wave, not only because it is weaker due to its propagation in the same direction as the outflowing current but also because of the deeper surface layer depth.

The first scientific question addressed in this paper is to show that extreme tidal internal waves are observed only over the sill, while elsewhere in the strait they are weaker. The second objective is to determine the parameters of internal tides in the strait on the basis of moored measurements and numerical calculations. The third objective is to find the causes of the strong internal bore observed in the eastern part of the strait and to understand the role of the currents in the formation of the bore, which is seen in its surface manifestation.

This paper is organized as follows. Section 2 is devoted to the description of measurements over Camarinal Sill. In section 3 we estimate the wavelength and the direction of wave propagation. In section 4 we present the results of numerical modeling, which show the influence of different currents on internal waves.

2. Moored measurements

A map of the moorings deployed in the Strait of Gibraltar during the 1985–86 Gibraltar experiment is shown in Fig. 1. The moorings without the suffix ''B'' were operating from October 1985 to May 1986, while those with the suffix were operating from May 1986 to October 1986. We used the data from buoy 2B to study the vertical structure of internal tidal oscillations since the vertical span of the instrument array at this buoy was the greatest. The current meters were located at depths 91, 112, 135, 182, 235, and 302 m. They also carried the conductivity and temperature sensors. Because of strong mean and tidal currents the instruments suffered large vertical displacements. For example, the instrument originally set at 91 m moved within a vertical range from 91 to 170 m. The instrument set at 112 m could deepen to 186 m, and so on. The mooring was set almost at the crest of the sill. The instruments were supplied with pressure sensors and, hence, we managed to trace the real location of the isotherms and analyze their temporal displacement by interpolating the tem-

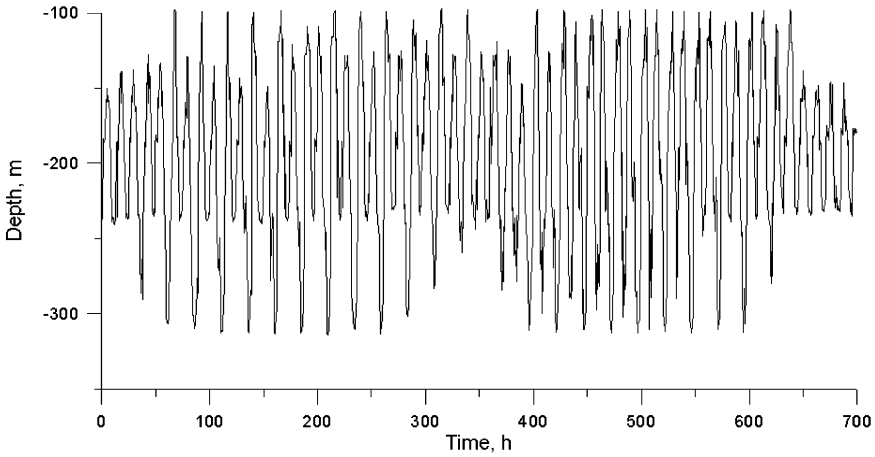

FIG. 2. Depth variation of the 13°C isotherm from 2 to 31 Jul 1986.

perature values to the fixed levels of depth. The time sampling was 30 minutes. Knowing the depth of the instrument and the temperature measurement at each sampling for each of the six instruments we calculated the depth of several isotherms. Displacement of the 13°C isotherm gives the best thermal pattern. Its vertical displacement ranges from 100 to 300 m (Fig. 2) so that its depth variation from 2 to 31 July 1986 (shown in the figure) falls within the depth interval covered with instruments.

There were only one or two instruments on the buoys set east (buoy 7) and west (buoys 4 and 8) of the sill. We cannot use the same procedure to estimate the amplitudes of vertical displacements on these buoys. Here, we estimated the vertical displacements comparing the minimum and maximum temperatures measured by the instruments during 12-h fluctuations with the mean vertical distribution of temperature. We also used this method to estimate the vertical displacements at buoy 2 to determine the error of our estimations. The method of comparing the maximum and minimum temperatures with the vertical temperature profile gave an average error of 5%, while the maximum error did not exceed 8%. A very important fact is that, unlike buoy 2, the instruments at buoys 7, 4, and 8 were not subject to strong vertical displacements and the vertical motion of the instruments did not exceed 2–3 m. Estimates of the amplitude of vertical displacements at buoys 4, 8, and 7 shows that they are 3–4 times smaller than on buoy 2 set near Camarinal Sill.

TABLE 1. Band filtering parameters for four tidal components.

Tidal component	Period (h)	Low frequency (h^{-1})	High frequency (h^{-1})	Mean amplitude (m)
S_2	12.00	1/12.05	1/11.95	12.69
M_2	12.42	1/12.47	1/12.37	68.80
K_1	23.93	1/24.11	1/23.73	22.56
O_1	25.82	1/26.02	1/25.63	18.91

We used a band filter to separate different tidal components forming internal oscillations over the sill mapped by the time series of the 13°C isotherm depth. The time series with 0.5-h sampling time were band filtered using a second-order elliptic filter (Parks and Burrus 1987). To isolate the fluctuations with M_2 frequency we provided a frequency band between 1/12.37 and 1/12.47 h^{-1} tuned to a semidiurnal frequency of 1/12.42 h^{-1}. Similar parameters were used to isolate the oscillations with other tidal frequencies. The parameters for band filtering of tidal components are given in Table 1.

Graphs of fluctuations with the frequencies of the main tidal components are shown in Fig. 3. The mean amplitudes of internal fluctuations are given in the last column of Table 1. The superposition of diurnal and semidiurnal tidal components is visually seen in Fig. 2. The amplitude of the isolated internal wave with a period of 12.42 h (M_2) only slightly changes with time. The other components are characterized by a greater variability of their amplitudes, which can be explained by the errors in the procedure of their determination from measurements and nonideal filtering. The strong signal associated with the M_2 internal tide is less subject to errors. The signal with the S_2 frequency is influenced by the strong M_2 signal, and filtering cannot eliminate the beating seen in the figure.

Bryden et al. (1994) gave a 30-day variation of the interface based on moored salinity measurements. The pattern of fluctuations is similar. Conductivity measurements on buoys are subject to a bias toward high (unrealistic) salinities and temporal drift to fresher values (see Fig. 3 from Bryden et al. 1994). Hence, conductivity correction is needed, which may give errors in calculating salinity and density. We consider that temperature is a better tracer than salinity or density because no corrections are needed for temperature measurements. MacDonald et al. (1994) compared the monthly mean moored temperatures with monthly mean tem-

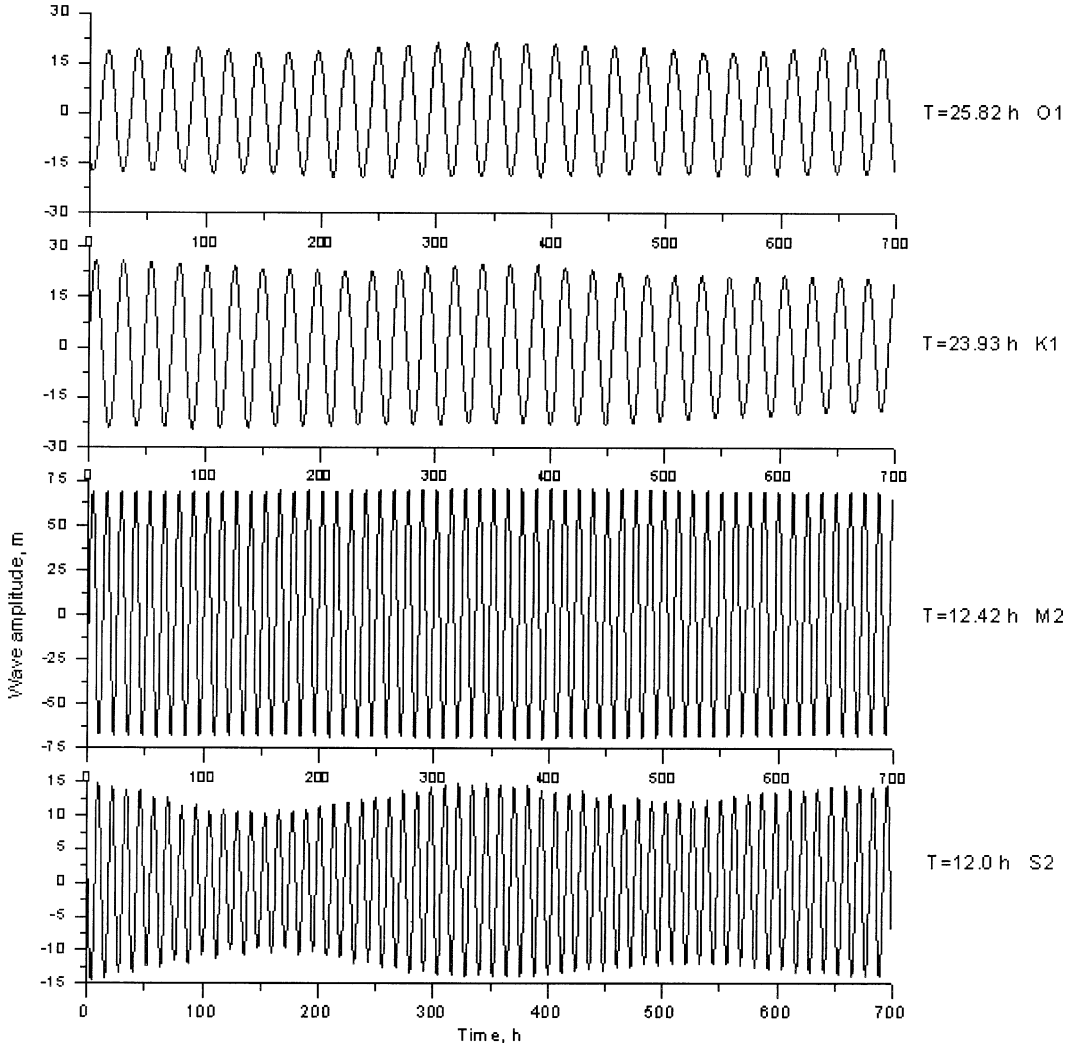

FIG. 3. Graphs of vertical displacements with the frequencies of the main tidal components from 2 to 31 Jul 1986, after band filtering.

peratures from the temperature atlas. The results were in good statistical agreement. Their calculations of heat transport through the strait based on moored temperature and velocity measurements provide a realistic balance of the heat budget in the Western Mediterranean.

The amplitudes of internal tide at Camarinal Sill are strong because we observe these waves immediately in the region of their generation over the slopes of bottom topography, where the barotropic tidal currents force internal oscillations. Further evidence that the waves observed over Camarinal Sill are forced waves comes from the correlation between the temperature and velocity time series. Figure 4 illustrates the time series of temperature, velocity, and depth of the 13°C isotherm measured at buoy 2B over the sill. The time series of temperature and velocity were measured with an instrument located at a minimal depth of 135 m. The correlation is very high, and we see that the maxima of positive horizontal velocity (eastward) approximately coincide with the maxima of temperature and minima of the isotherm depth. This is to be expected because the mooring was located almost at the top of the sill, and the streamlines periodically flow over the sill rising over one slope and sinking over the other. The instrument measures the horizontal velocity of currents caused mostly by the barotropic tide, while these currents induce temperature oscillations, which appear due to vertical displacements.

3. Wavelength and direction of propagation

To estimate the wavelength of the semidiurnal waves we used the antenna method developed in seismology and applied to oceanic waves by Barber (1963) assuming arbitrary position of the wave sensors. The method is based on the calculation of cross-spectra for each pair

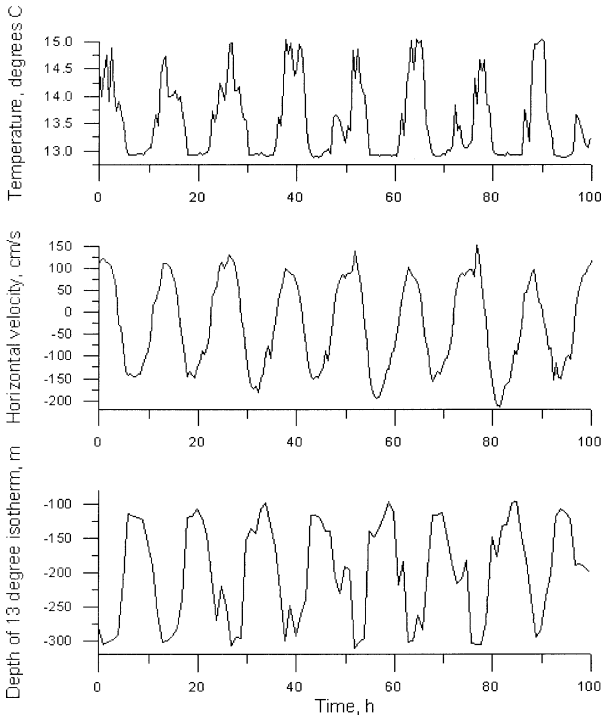

FIG. 4. Time series of temperature and horizontal velocity, measured over the Camarinal Sill on buoy 2B at 135 m, and time series of the 13°C isotherm obtained by interpolation of temperature measurements at each of the instruments.

of the possible combinations of sensors with further convolution at the frequency of the waves under study. The amplitude and phase cross-characteristics of the oscillation are used to calculate the spatiotemporal spectra at the wave frequency and estimate the components of the horizontal wavenumber. The method basically accounts for the statistical phase difference between each pair of wave sensors. In our case we used the temperature sensors, which indicate the vertical motion induced by internal waves, assuming that the vertical gradients of temperature are significant. It is important that the distance between the moorings be comparable with the wavelength of the oscillations under study. Otherwise uncertainty appears in the interpretation of the phase differences if the distance between the sensors is too large. If the distance between the sensors is two small and the span of the array of sensors is smaller than the wavelength due to a limited number of sensors, it is impossible to resolve the wavelength correctly.

The calculation of spatiotemporal spectra at semidiurnal frequency was carried out using the following formula:

$$E(k_x, k_y, f_0) = 2 \sum_{i=1}^{n-1} \sum_{j=i+1}^{n} [P_{ij}(f_0) \cos 2\pi(k_x x_{ij} + k_y y_{ij}) - Q_{ij}(f_0) \sin 2\pi(k_x x_{ij} + k_y y_{ij})], \quad (1)$$

where $k_x^2 + k_y^2 = k^2$ is the spatial wavenumber, while the wavelength L is $L = 1/k$; i, j are the sequential numbers of the sensors; n is the total number of the sensors; P_{ij} and Q_{ij} are the real and imaginary parts of the cross-spectrum between the sensors with numbers i and j; $x_{ij} = X_i - X_j$ and $y_{ij} = Y_i - Y_j$ are the projections of the distances between the sensors on the horizontal axes x and y.

We did not have many moorings to estimate the spatial characteristics of the waves. Assuming that the main generation of tidal internal waves occurs at Camarinal Sill, the moorings in the strait can be divided into two groups. As we are interested in the signal associated with internal motion, we used only the temperature sensors at the moorings to make the calculations because strong barotropic tidal currents superimposed on internal tidal oscillations would require preliminary separation. The first (western) group of sensors, which allows us to measure the waves propagating to the west of the sill, includes moorings 1, 2, 3, 8, and 4 in the first interval of observations, and moorings 2, 3, and 4 in the second interval. The second (eastern) group of buoys includes moorings 1, 2, 3, and 7 in the first interval and moorings 2, 3, 9, and 7 in the second interval. Note that at least three moorings located in the form of a triangle are needed to estimate the wavelength and the direction of the wave propagation, although three sensors do not permit enough wavenumber resolution. The records at moorings 2 and 4 in the first period of observations were only 31 and 17 days long, respectively. Thus, we did not have enough information to calculate the parameters of the waves after the end of the records at these moorings. In addition the depths of measurements were different between them and they were not constant due to the strong tilt of the whole mooring system induced by strong currents. There were very few buoys in the experiment; consequently these calculations are very rough and give only approximate values of the wave parameters.

We made calculations of the cross-spectra over different intervals of observations, from two weeks to one month, both for the total number of moorings at each side of the sill and various combinations of moorings. The results based on 10 different combinations of the duration of time series and number of the moorings for the western group are as follows: The wavelength ranges from 45 to 60 km, and the azimuth direction of the wave propagation changes between 210° and 280° indicating that wave propagates to the west.

The wave propagating to the east of the sill was estimated on the basis of 16 different combinations of buoys and the duration of the time series. The wave generally propagates to the east in the azimuth interval between 90° and 120°, while the wavelength ranges between 90 and 140 km. The difference between the wavelengths in the western and eastern parts is not surprising because the depths of the strait east of Camarinal Sill are greater than in the western part of the strait.

The previous analysis dealt with the time series, which were less than one month. The duration of this time series did not allow us to separate the M_2 and S_2 peaks (12.4 and 12.0 h). The measurements with a greater duration (5 months) were obtained only at three moorings from each side of Camarinal Sill and could not provide good spatial resolution. The phase differences between the time series at M_2 and S_2 frequencies did not differ greatly, which indicates that the wavelengths of these waves are very close.

Wavelength of the internal tide can be also estimated on the basis of the dispersion relation. We assume that these calculations are valid if the bottom is flat and no forcing exists beyond the slopes of the sill. We can estimate the wavelength of the internal tide by numerical integration of the equation for vertical velocity (w) caused by internal waves with zero boundary conditions at the surface and bottom:

$$\frac{d^2w}{dz^2} + \frac{N^2(z)}{g}\frac{dw}{dz} + \frac{N^2(z) - \omega^2}{\omega^2 - f^2}wk^2 = 0, \qquad (2)$$

where $N^2(z)$ is the Brunt–Väisälä frequency based on CTD data east and west of the sill, ω is the semidiumal frequency, f is the Coriolis parameter, and k is the horizontal wavenumber. We integrated this equation with a vertical step of 10 m for typical stratification east and west of the sill. The wavenumbers obtained in the solution of this eigenfunction problem correspond to the modes of internal tides. We can judge the mode number by the number of zero crossings of the eigenfunction. Mode one has no zero crossings (only zero values at the bottom and surface), mode two has one zero crossing, etc. We assumed the mean depth east of the sill is equal to 800 m and west of the sill it is equal to 450 m. The calculated wavelength of the semidiurnal internal tide (mode one) east of the sill was 94 km (phase velocity 2.1 m s^{-1}), and west of the sill the wavelength was equal to 58 km (phase velocity 1.3 m s^{-1}). These values for the first mode agree with the estimations made with the spatiotemporal spectrum and observations of the surface manifestation of internal tides. The wavelength difference between the eastern and western parts of the strait accounted for greater stratification and depth in the eastern part, which favor longer internal tidal waves. Phase velocity of the baroclinic tide is significantly lower than the barotropic wave velocity estimated as $C = \sqrt{gH}$. The velocities of the barotropic tide are 80 and 90 m s^{-1} in the western and eastern parts of the strait, respectively, as compared with 1.3 and 2.1 m s^{-1} for the velocity of the internal tidal wave in the western and eastern parts.

4. A model calculation

Many models exist that describe the generation of internal tides over the sill (Hibia 1990; Longo et al. 1992; Wang 1993). The model of Brunt et al. (1996) describes internal tide in terms of the interface displacement. This model describes the generation and evolution of a tidal internal wave and its transformation into a series of internal waves with shorter periods. Wang (1993) uses a model for continuous stratification, but the resolution of the model is too coarse to analyze the propagation of short-period wave packets. The model of Longo et al. (1992) is a nonlinear two-layer model assuming the water stratification as two layers of varying thickness, while internal oscillations are generated at the interface between the layers. Their model reproduced internal solitary waves observed in the Alboran Sea. We think that reducing the internal motion only to the displacement of the interface or the pycnocline is not enough for the analysis of tidal internal waves. For high-frequency internal waves or solitary waves the pycnocline may be the waveguide (Derzho and Velarde 1995), but unlike the interface between the layers, the pycnocline influences the properties and parameters of the propagating internal waves. Stratification in the Strait of Gibraltar allows for the internal motion with a semidiurnal period in the entire water column with a maximum vertical displacement at middle depths close to the thermocline decreasing to the surface and bottom. We use a fully nonhydrostatic model with continuous stratification, which could account both for the generation of internal waves over bottom topography and the description of their propagation and evolution. The density profiles of Atlantic and Mediterranean waters specified in the model are shown in Fig. 5.

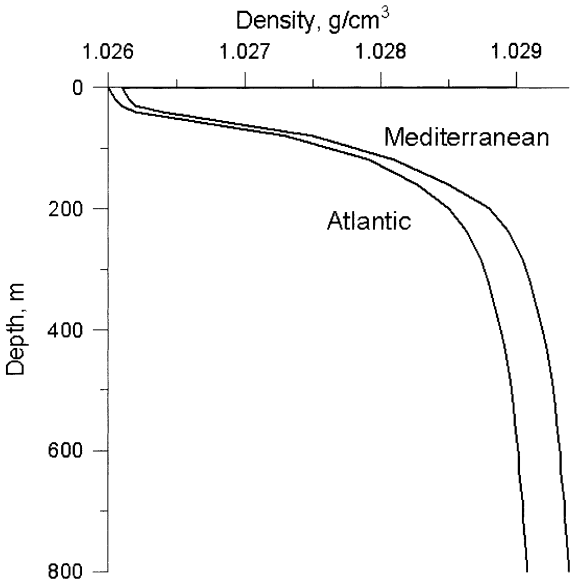

FIG. 5. Density profile of Atlantic and Mediterranean waters specified in the model.

In particular, we consider a two-dimensional (x, z) flow in a continuously stratified rotating ocean of variable depth. Then, internal waves are described by the following set of equations:

$$\Omega_t + J(\Omega, \Psi) - fV_z = \frac{g\rho_x}{\rho_0} + K(x)\Omega_{xx} + K\Omega_{zz} + (K\Psi_{zz})_z$$

$$V_t + J(V, \Psi) + f\Psi_z = K(x)V_{xx} + (KV_z)_z$$

$$\rho_t + J(\rho, \Psi) + \frac{\rho_0 N^2(z)}{g}\Psi_x = R(x)\rho_{xx} + (R\rho_z)_z + (R\rho_{0_z})_z, \quad (3)$$

where Ψ is the streamfunction ($\Psi_z = u$; $\Psi_x = -w$); $\Omega = \Psi_{xx} + \Psi_{zz}$ is the vorticity; (U, V, W) is the velocity vector; N is the Brunt–Väisälä frequency; ρ is the density disturbance due to the wave motion; ρ_0 is the mean density; f is the Coriolis parameter; K, $K(x)$, R, and $R(x)$ are vertical and horizontal coefficients of turbulent viscosity and mass diffusivity; J is the Jacobian; and g is the acceleration due to gravity.

Although the model is two-dimensional, we introduce the equation for the V component of velocity normal to the x, z plane to account for the effects of rotation. However, the V component is considered constant. For convenience, the equation of density diffusion has been used instead of the equations of heat and salt diffusion.

The boundary conditions at the surface located at $z = 0$ are

$$\rho_z = 0, \qquad \Omega = 0, \qquad \Psi = 0, \quad (4)$$

and hence, no tangential stresses are considered. We also consider zero vertical motion and no heat and salt transport through the surface.

At the bottom no heat, salt, and mass transports exist:

$$\text{at } z = -H(x), \qquad \partial\rho/\partial\mathbf{n} = 0, \qquad \Psi = \Psi_0 \sin\omega t, \quad (5)$$

where ω is the tidal frequency, $\mathbf{n}$ denotes the unit normal vector to the bottom, and Ψ_0 is the amplitude of the mass transport in a barotropic tidal current. The boundary condition for vorticity at the bottom is calculated using $\Omega = \Delta\Psi$ with the value of the Ψ field obtained at the previous time step.

The wave perturbations of vorticity, streamfunction, and density are assumed zero at the lateral boundaries located far from the bottom irregularities at the submarine ridge. We stop the calculations when the wave perturbations reach the lateral boundaries. The phase velocity of the perturbations does not exceed 2–3 m s^{-1}, which allows us to continue the calculations for a suitable number of time steps.

The calculations start from a state of rest when the fluid at the bottom is motionless and the isopycnals are horizontal; hence at $t = 0$: $\Omega = 0$, $\rho = 0$, $\Psi = 0$.

The bottom topography was introduced in the model from the data of navigation charts. Continuous stratification was specified with the values of Brunt–Väisälä frequency in each of the 20 layers calculated on the basis of CTD profiling.

The vertical step in the model varies with depth, but the number of levels is equal to 20 and does not change with the changing depth. The thickness of the layers is reduced in the depth intervals with strong stratification and increased, where the stratification is weak, by introducing a new variable:

$$z_1 = \int_0^z N(s)\, ds \Big/ \int_0^{-H(x)} N(s)\, ds, \quad (6)$$

where z_1 is a new variable describing depth, z is the old depth variable, $N(s)$ is the depth-dependent Brunt–Väisälä frequency, s is a dummy variable for differentiating by the vertical to the current depth level, and $H(x)$ is the depth of the ocean. This transformation allows us to convert a curvilinear grid, caused by irregular bottom topography, to a rectangular one (the new coordinates are termed σ coordinates). After the end of calculations we make a back transformation to present the results in the usual form.

A semi-implicit numerical scheme utilizes a rectangular grid with second-order approximations to the spatial derivatives and first-order approximation of the temporal derivatives in every temporal semilayer. At each time step, the implicit system, which is a tridiagonal matrix, is solved using standard techniques.

We have chosen a domain 300 km long with a horizontal step of 200 m and 20 vertical levels. The horizontal size of the domain significantly exceeds the size of the strait, but allows us to analyze the processes in the middle of the domain before the perturbations reach the lateral boundaries. The time step was approximately equal to 7 s. These parameters satisfy the Courant–Friedrichs–Levy condition (Richtmyer 1957). The coefficients of the horizontal eddy viscosity and density diffusivity were fixed to 60 m^2 s^{-1} over the ridge and 4 m^2 s^{-1} beyond the ridge over the flat bottom in the model. Strong motion over the slopes of the sill requires large values of the coefficients. This choice of the spatial and time steps together with the choice of the coefficients of turbulent viscosity allowed us to make the calculations free from numerical instability caused by the strong nonlinearity induced by the enormous tidal transport along the strait. The values of the horizontal eddy viscosity and density diffusivity in the numerical calculation were minimized to eliminate numerical instability. Smaller values of turbulent viscosity and density diffusivity lead to instability. The coefficients of vertical turbulent viscosity and density diffusion were set to 0.001 m^2 s^{-1}, but their role was not very important.

The main objective of the model investigation is to study the influence of the currents on internal tide propagation in the strait. In the first version of model calculations we make the approximation of the model with zero mean current. We introduce only a periodical barotropic tidal flow by periodical increasing and decreasing the value of the streamfunction at the surface, while the streamfunction at the bottom is specified equal to

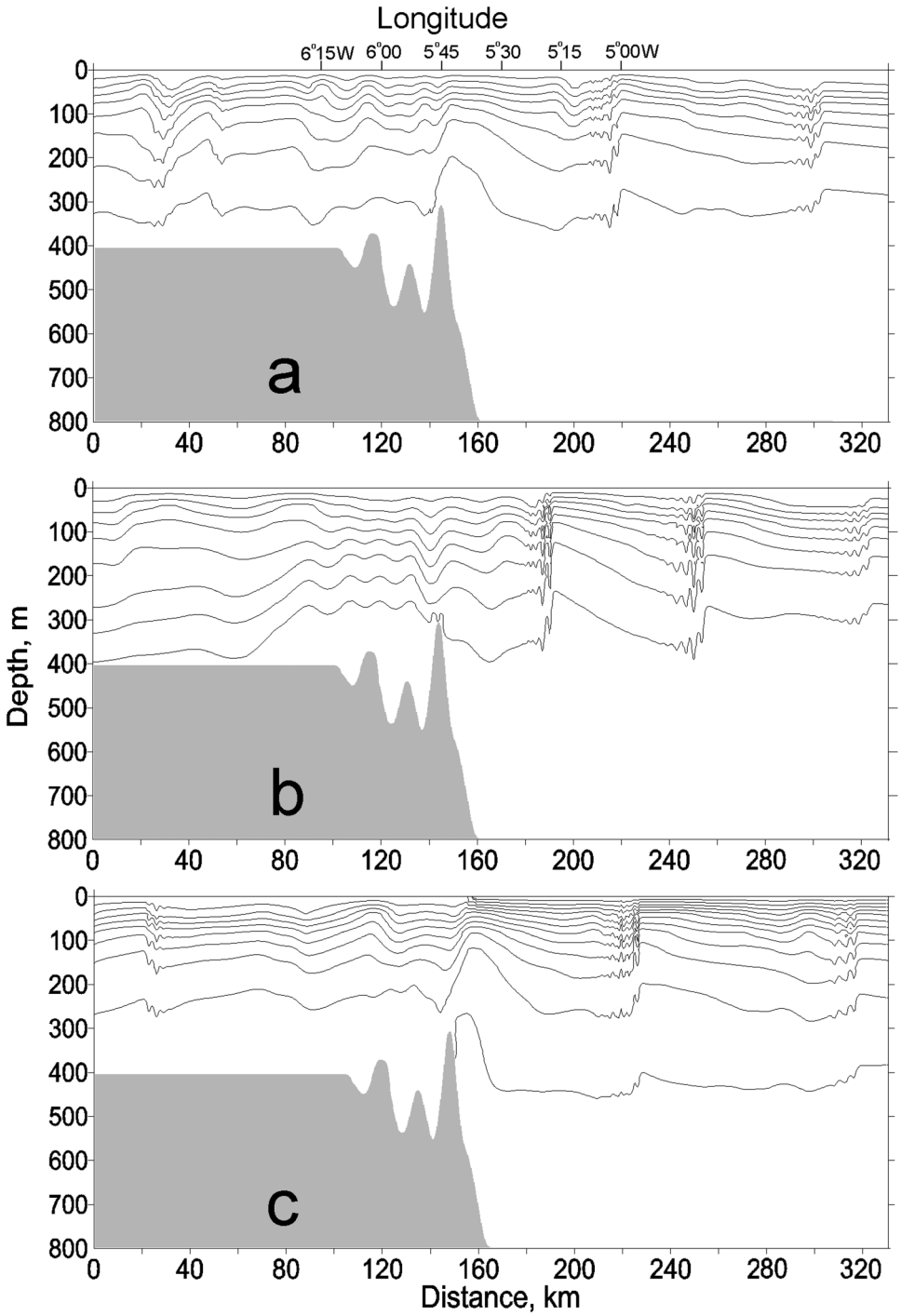

FIG. 6. Perturbations of the density field induced by a propagating internal tide. The contour lines of density are shown with an interval of 0.000 25 g cm^{-3}. The gray-colored pattern shows bottom topography. The density perturbation develop on the background of different currents in the strait: (a) zero mean current, (b) westward barotropic current, and (c) oppositely directed inflowing and outflowing currents.

zero. The maximum value of the streamfunction was chosen to provide maximum horizontal tidal velocities equal to 80 cm s^{-1}. The period of reciprocating flow is 12.4 h.

The periodic changes in the horizontal flow induce an internal wave propagating in both directions from a sill positioned in the middle of the computation area. Perturbations of the density field induced by propagating internal tide are shown in Fig. 6a. This snapshot of the density field is depicted after four tidal periods. The

fluctuations of the density field are not symmetrical with respect to the position of the Camarinal Sill. The bottom topography is also not symmetrical. Camarinal Sill is strongly abrupt at the eastern slope, while the bottom topography is more corrugated and the mean inclination of the slope is smaller west of the sill. A calculation, when the bottom topography was specified only by a symmetric sill, gave a symmetric pattern of propagating fluctuation in both directions from the sill.

The interaction of the barotropic tide with the bottom topography induces stronger internal tide propagating to the east in comparison with that propagating to the west. Camarinal Sill is the major source of internal tide generation because it is closer to the density interface. The waves generated over bottom topography west of Camarinal Sill partly damp the internal tide generated over the western slope of Camarinal Sill.

An internal bore is formed on the trailing edge of the wave, which is steeper than the leading edge. A packet of shorter internal waves follows the bore. The structure of the westward-propagating wave is the same except that the bore and wave train of shorter internal waves are less intense in the western part in comparison with the eastern part of the basin.

In the second version of model calculation we introduce a steady barotropic westward current in the entire water column of the strait by specifying the permanent value of the streamfunction at the surface and zero at the bottom so that the velocity of the mean current is equal to 30 cm s^{-1} at the western boundary. At the eastern boundary the velocity is equal to 18 cm s^{-1}. The mean velocity over the sill is equal to 41 cm s^{-1}. We superimpose a periodical barotropic tidal current on the mean current as done in the previous step. At the western boundary, the maximum amplitude of the barotropic tidal velocity is 80 cm s^{-1}, the same as it was without the mean current.

The westward flow changes the internal wave field (Fig. 6b). In the eastern part, where the internal tide propagates opposite to the current, we observe a well-pronounced internal bore followed by a train of short-period internal waves. A mean current opposing the wave makes the wavelength shorter, and hence the slopes of the internal tide are steeper, which leads to wave breaking and formation of a packet of shorter internal waves. For a uniform westward current the bore is observed in the entire water column.

West of Camarinal Sill the internal tide propagates in the same direction as the outflowing current. The current increases the wavelength. The internal bore is formed, but only a weak packet of shorter waves appears.

In the third version of the model calculation we have analyzed the internal tide developing in the strait with two opposite currents, modeling the real situation. The eastward flow with mean velocities of 50 cm s^{-1} occupies the upper layer of 250–300 m and the lower current with a vertically average velocity of 25 cm s^{-1} occupies the rest of the water column. These two opposing flows yield a strong shear at depth 200 m. The two oppositely directed currents in the stream were introduced in the model by specifying two different vertical distributions of density in the eastern and western parts. In this version of calculations the computational area was increased in the eastern and western directions. In the beginning of the calculations the water was set to flow free under the influence of different density distributions in the eastern and western parts. After adjustment and formation of a two-layer flow in the central part of the computational area we superimpose the same tidal flow as in the previous versions of calculations. The wavelength of the easterly propagating wave is 90 km. The leading edge of the wave is flatter than the trailing edge, which is very steep. This leads to the formation of an internal bore. A train of shorter internal waves follows a sharp depression of density contours. The westward-propagating wave is shorter. Its wavelength is 60 km, as the depth west of Camarinal Sill is smaller. The structure of the wave is approximately the same except that the internal bore is less intense in the western part than in the eastern part of the basin.

The introduction of two opposite currents with a shear intensifies the internal bore in the upper layer at depths of 100–200 m, while in the deeper water it becomes less apparent (Fig. 6c). Intensification of the internal bore and associated short period internal waves in the upper layer in the eastern part obtained in the model calculations confirms the observations at the surface made from satellites, airplanes, and coastal radars that surface manifestations of internal tide are clearly seen in the eastern part of the strait.

Numerical calculations of isopycnal fluctuations in the main thermocline demonstrating the formation and propagation of the internal bore are shown in Fig. 7. The direction of the barotropic tidal currents and time of low and high water are indicated on the right side of the wave patterns. We present seven sequential snapshots of the location of isopycnals with an interval of two hours, which cover a tidal period. The regime of internal waves propagating to the west (in the same direction as the outflowing current) and those propagating to the east differs significantly. Internal waves propagating eastward have a greater amplitude, which

→

FIG. 7. Evolution of density perturbations during a tidal period. Contours are shown with an interval of 0.000 25 g cm^{-3}. The patterns are plotted at an interval of 2 h. The time intervals are given with respect to the semidiurnal tidal period (T = 12.4 h). Initial time (t = 0) corresponds to zero velocities of the barotropic tide along the strait. The time moments of low and high water and the direction of the barotropic tide are shown near the patterns.

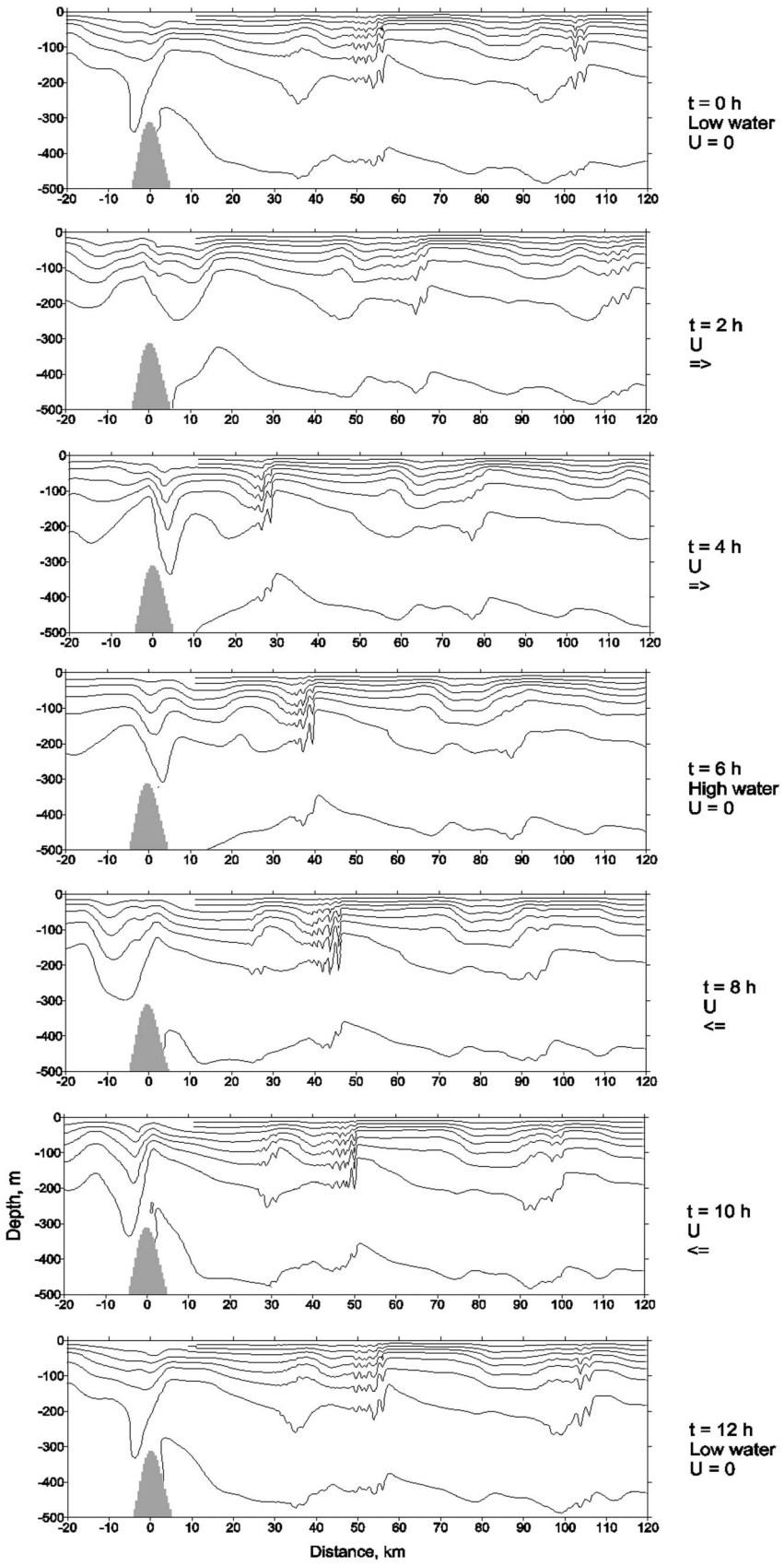
t = 0 h
Low water
U = 0
t = 2 h
U
=>
t = 4 h
U
=>
t = 6 h
High water
U = 0
t = 8 h
U
<=
t = 10 h
U
<=
t = 12 h
Low water
U = 0
Depth, m
Distance, km

agrees with the theory of wave trapping by the currents, when the current vector and the vector of the phase velocity of the waves are opposite to each other (Ivanov and Morozov 1974; Badulin et al. 1985). The waves propagate in the direction opposite to the currents like a periodical pulse of internal tidal perturbations, which rapidly increases its amplitude and then breaks into a packet of shorter internal waves. Initially, the amplitude of vertical displacements caused by internal waves exceeded 100 m. It decreases while the wave propagates away from the sill, and small-scale internal waves developing at the steep slopes of isopycnals associated with undular internal bores are generated. These short internal waves with a wavelength of about 7–8 km develop on the trailing edge of the propagating tidal internal wave. They absorb energy from the internal tide and propagate in the same direction with approximately the same speed as the main wave carrier. A packet of short-period internal waves starts to form east of the sill before high water when the eastward-directed barotropic current decreases. After high water, the barotropic tidal current reverses toward the west and decreases the velocity of the eastward-propagating internal tide. This compresses the wave packet and intensifies it. Several hours later after low water, when the current direction coincides with the propagation of the wave packet, the latter becomes longer, the amplitudes of the waves in the packet decrease, and its leading edge propagates faster. The speed of the leading edge changes from 0.8 to 1.6 m s^{-1} depending on the relative velocity of the barotropic flow. One can observe that an undular bore also propagates to the west, but here it is weaker than on the eastern side.

To compare our model numerical results with observations we show a graph of the evolution of isopycnals at a point near the top of the sill calculated from the model. The density values from the corresponding vertical line of the model grid were recorded for each time step coinciding to a one-hour interval (1/12 tidal period) of real time. Thus, we get a result reproducing the oscillations of the isotherm shown in Fig. 2 except for the fact that in the model we deal with density, while in reality we take temperature records as tracers. The calculated oscillations of the isopycnal corresponding to the density 1.0285 g cm^{-3}, which is similar to the 13°C isotherm, are shown in Fig. 8.

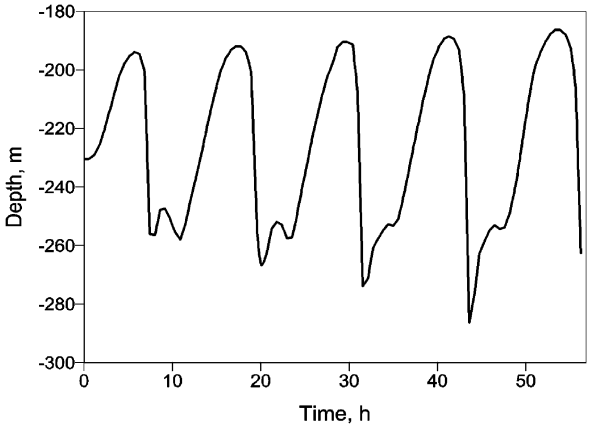

FIG. 8. Oscillation of the 1.0285 g cm^{-3} isopycnal based on the numerical calculations on a vertical grid line close to the crest of the sill.

5. Discussion

We have analyzed the current and temperature measurements in the Strait of Gibraltar obtained from moorings deployed on Camarinal Sill and at both sides of the sill. The observations indicate that internal tides generated over the sill are very intense with vertical peak-to-peak displacements sometimes exceeding 200 m. We observe these oscillations over the sill exactly at the source of their generation and conclude that these waves are forced internal oscillations, which transform into a free propagating wave, east and west of the sill. These extreme waves rapidly lose their energy and at a distance of approximately 50 km from the sill their amplitude becomes 3–4 times smaller. Internal tidal waves include four main tidal components similar to the components of the barotropic tide (M_2, S_2, O_1, K_1). Among these the M_2 (12.4 h) component is the strongest with an amplitude of almost 70 m. The waves propagate along the strait in a stratified shear flow, where the upper layer with a thickness of 150–200 m moves eastward, while the major part of the water column propagates to the west.

Internal tidal waves occupy the entire water column. Since the outflowing current in the lower part of the water column is thicker than the surface inflowing current and the maximum of the first mode of the internal tide is located in the outflowing current, the interaction of the wave with the outflowing current is more important.

In the eastern part of the strait oppositely directed vectors of current and wave account for the concentration of wave energy at a smaller spatial scale with an increase in wave amplitude. This leads to wave breaking and formation of an undular internal bore on the trailing edge of the wave, while the leading edge becomes flatter. The packets of short-period internal waves, which follow the bore, are clearly seen at the surface because the thermocline east of the sill, where they develop, rises close to the surface. The mean stratification and depth in the eastern part of the strait determine the conditions for wave propagation with a wavelength of approximately 90 km. This value was calculated from the mooring data. Model calculations give approximately the same value. West of the sill the situation is opposite. The wave propagates in the same direction as the outflowing current. This decreases the amplitude of the wave, while the shallower depths west of the sill constrain the wavelength to about 60 km. West of the sill, the pycnocline is deeper, and the undular bore is not

TABLE 2. Wavelengths of semidiurnal internal tides determined by different methods relative to top of the sill.

	West (km)	East (km)
Measured on a mooring array	45–60	90–140
Calculated from dispersion relation	58	84
Calculated using the numerical model	60	90

formed in the same way as observed east of the sill. Evidence from surface observations is scarce. The wavelengths of semidiurnal internal tides in the western and eastern parts of the strait are given in Table 2.

Intense internal wave breaking causes mixing of water within the pycnocline. This leads to an increase in the pycnocline thickness west of the sill thus increasing the potential energy of the water column of the outflowing water, which can be accounted for by the energy losses of tidal internal waves estimated from the difference of their amplitudes. This favors the assumption that tidal internal wave breaking is responsible for the intensive exchange between the upper and lower layers in the Strait of Gibraltar. Mixing east of the sill is apparently greater than west of the sill because the former is induced by internal waves of greater energy together with the undular bore propagating along the trailing edge of the wave.

The multilayer numerical model used to calculate the generation and propagation of internal tides in the strait confirmed observed properties of the internal tide. Modeling results show the formation of an undular bore east of the sill and a weak undular bore west of it. The wave parameters obtained in the model are in good agreement with the field observations earlier reviewed in the paper. They also correlate with observations of the spatial periodicity of the internal bore observed in the eastern part of the strait. The model with continuous stratification better reproduces internal tide properties and wave breaking than two-layer models. The model shows the important role of the outflowing current in forming the undular bore. A strong shear between oppositely directed currents intensifies the bore and wave packet in the upper layer. This confirms the fact that observations of surface manifestations of the internal tide are better expressed in the eastern part of the strait.

Our analysis gives an answer as to why internal waves observed at Camarinal Sill are significantly greater than in the other parts of the strait, where they are smaller but strong enough to provide significant mixing of the two water layers. Camarinal Sill is the main source of internal tide generation. The waves propagate east and west of the sill and lose their energy.

In addition to internal waves propagating along the strait, there is evidence of high-frequency waves propagating across it. These waves are seen on photographs from space and radar images (Farmer and Armi 1986; DAAC/NASA 1996; Richez 1994; Watson and Robinson 1990). Their wavelength is about 1 km, and the period is about 0.25 h. Very frequently, transverse waves can be recognized as those generated near the capes and propagating off the cape. Such waves were detected by radar measurements, and it is likely that they were emanating from Cape Ciris. The other packet of waves was seen propagating from Ceuta. These waves might be formed in a supercritical flow through an open channel (Henderson 1966; Watson 1994). Nonlinear transfer of wave energy from longitudinal to transversal modes in a channel was studied by Trulsen et al. (1999) based on a laboratory model.

The energy of tidal internal waves propagating along the strait can be transmitted to transversal waves by a mechanism based on the interaction of the waves propagating along the strait with transversal perturbations of bottom topography close to the capes. These waves may also be generated by irregularities in the strait, which in turn generate waves whenever there is an unsteady flow past them. In addition, the generation can occur because of the onshore and offshore motion of water induced by wind or currents, which cause periodical displacements of water over the inclined bottom near the shore. These waves can also be caused by the perturbations and refraction of the internal bore over the bottom topography close to the coastline. The perturbations of the current in the upper layer may be induced by the undular bore, which has approximately the same periodicity.

6. Conclusions

The main results of this research are the following.

Internal tidal oscillations observed in the strait are mostly generated over Camarinal Sill.

The observations analyzed depict the generation of internal tides with peak-to-peak amplitudes exceeding 200 m. The waves propagate in both directions from the sill loosing energy while propagating. The major motion of internal tide is associated with the semidiurnal M_2 frequency.

The wavelength of the waves propagating to the east is somewhat greater than for the waves propagating to the west because of the relative difference in the depth of the strait and greater stratification in the eastern part of the strait.

Internal tides propagating to the east in the opposite direction to the lower current in the strait are accompanied with an internal bore and packets of short-period waves, which can be identified at the surface. Strong shear between the oppositely directed currents intensifies the bore in the upper layer.

The undular bore formed by the interaction of an internal tide with the currents is better manifested in the eastern part of the strait. This bore and the accompanying packet of shorter internal waves are the main and evident surface indication of the internal tide. This fact gives additional explanation to why some of the observations, made mostly by remote observation of the sur-

face, support the idea that internal tides exist only in the eastern part of the strait.

Acknowledgments. The authors are grateful to G. Parrilla and H. Bryden for enlightening discussions, correspondence, and many suggestions that helped improved our understanding of the problem. Useful remarks made by three anonymous referees are also gratefully acknowledged. The data of moored measurements were taken from the WOCE Current Meter Data Assembly Center in Oregon State University. This research was supported by DGICYT (Spain) under Grant PB 96-599, by the European Union under a fellowship Grant MAS3-CT96-5016, and under TMR Programme Network Grant ERBFMRXCT96-0010.

REFERENCES

Armi, L., and D. M. Farmer, 1988: Flow of Mediterranean water through the Strait of Gibraltar. *Progress in Oceanography*, Vol. 21, Pergamon, 1–105.

Badulin, S. I., V. I. Shrira, and L. S. Tsimring, 1985: The trapping and vertical focusing of internal waves in a pycnocline due to the horizontal inhomogeneities of density and currents. *J. Fluid Mech.,* **158,** 199–218.

Barber, N. F., 1963: The directional resolving power of an array of wave detectors. *Ocean Wave Spectra,* Prentice Hall, 137–150.

Bockel, M., 1962: Travaux oceanographiques de l' ''Origny'' a Gibraltar. *Cah. Oceanogr.,* **14,** 325–329.

Boyce, F. M., 1975: Internal waves in the Strait of Gibraltar. *Deep-Sea Res.,* **22,** 597–610.

Bray, N., C. D. Winant, T. H. Kinder, and J. Candela, 1990: Generation and kinematics of internal tide in the Strait of Gibraltar. *The Physical Oceanography of Sea Straits,* L. J. Pratt, Ed., Kluwer Academic, 477–491.

——, J. Ochoa, and T. H. Kinder, 1995: The role of the interface in exchange through the Strait of Gibraltar. *J. Geophys. Res.,* **100C,** 10 755–10 776.

Brunt, P., W. Alpers, and J. O. Backhaus, 1996: Study of the generation and propagation of internal waves in the Strait of Gibraltar using a numerical model and synthetic aperture radar images of the European ERS 1 satellite. *J. Geophys. Res.,* **101C,** 14 237–14 252.

Bryden, H. L., J. Candela, and T. H. Kinder, 1994: Exchange through the Strait of Gibraltar. *Progress in Oceanography,* Vol. 33, Pergamon, 201–248.

DAAC/NASA, 1996: Oceanography from the Space Shuttle, NASA photograph S-17-34-081. [Available from http://daac.gsfc.nasa.gov/CAMPAIGN_DOCS/OCDST/shuttle_oceanography_web/oss_cover.html.][Originally published by ONR in 1989.]

Derzho, O. G., and M. G. Velarde, 1995: Solitary waves of permanent form in a deep fluid with weak shear. *Phys. Fluids,* **7,** 1357–1362.

Farmer, D. M., and L. Armi, 1986: Maximal two-layer exchange over a sill and through the combination of a sill and contraction with barotropic flow. *J. Fluid Mech.,* **164,** 53–76.

——, and ——, 1988: Flow of Atlantic water through the Strait of Gibraltar. *Progress in Oceanography,* Vol. 21, Pergamon, 1–105.

Henderson, F. M., 1966: *Open Channel Flow*. Macmillan, 522 pp.

Hibia, T., 1990: Generation mechanism of internal waves by a vertically sheared tidal flow over a sill. *J. Geophys. Res.,* **95C,** 1757–1764.

Hopkins, T. S., 1978: Physical processes in the Mediterranean basins. *Estuarine Transport Processes,* B. Kjerve, Ed., University of South Carolina Press, 269–310.

Ivanov, Yu. A., and E. G. Morozov, 1974: Deformation of internal gravity waves by a flow with a horizontal velocity shear. *Oceanology,* **14,** 457–461.

Kinder, T. H., and H. L. Bryden, 1987: The 1985–1986 Gibraltar experiment: Data collection and preliminary results. *Eos, Trans. Amer. Geophys. Union,* **68,** 786–795.

Lacombe, H., and C. Richez, 1982: The regime of the Strait of Gibraltar. *Hydrodynamics of Semi-Enclosed Seas,* J. C. J. Nihoul, Ed., Elsivier, 13–74.

Lafuente, J. G., J. M. Vargas, F. Plaza, T. Sarhan, J. Candela, and B. Bascheck, 2000: Tide at the eastern section of the Strait of Gibraltar. *J. Geophys. Res.,* **105C,** 14 197–14 213.

La Violette, P. E., and R. A. Arnone, 1988: A tide-generated internal waveform in the western approaches to the Strait of Gibraltar. *J. Geophys. Res.,* **93C,** 15 653–15 667.

Longo, A., M. Manzo, and S. Pierini, 1992: A model for the generation of non-linear internal tides in the Strait of Gibraltar. *Oceanol. Acta,* **15,** 233–243.

MacDonald, A. M., J. Candela, and H. L. Bryden, 1994: An estimate of the net heat transport through the Strait of Gibraltar. *Seasonal and Interannual Variability of the Western Mediterranean Sea,* P. La Violette, Ed., Coastal and Estuarine Studies. Vol. 46, Amer. Geophys. Union, 13–32.

Monin, A. S., V. M. Kamenkovich, and V. G. Kort, 1974: *Variability of the World Ocean* (in Russian). Hydrometizdat, 262 pp.

Parks, T. W., and C. S. Burrus, 1987: *Digital Filter Design.* John Wiley and Sons, 340 pp.

Petigrew, N. R., and G. J. Nedell, 1989: Flow structure and variability in the Tarifa Narrows section of the Strait of Gibraltar. *Seminario Sobre la Oceanografia Fisica del Estrecho de Gibraltar,* J. L. Almazan et al., Eds., SECEG, 207–229.

Richez, C., 1994: Airborne synthetic aperture radar tracking of internal waves in the Strait of Gibraltar. *Progress in Oceanography,* Vol. 33, Pergamon, 93–159.

Richtmyer, R. D., 1957: *Difference Methods for Initial-Value Problems.* Interscience, 238 pp.

Trulsen, K., C. T. Stansberg, and M. G. Velarde, 1999: Laboratory evidence of three-dimensional frequency downshift of waves in a long tank. *Phys. Fluids,* **11,** 235–237.

Wang, D.-P., 1993: The Strait of Gibraltar model: Internal tide, diurnal inequality and fort-nightly modulation. *Deep-Sea Res.,* **40,** 1187–1203.

Watson, G., 1994: Internal waves in a stratified shear flow: The Strait of Gibraltar. *J. Phys. Oceanogr.,* **24,** 509–517.

——, and I. S. Robinson, 1990: A study of internal wave propagation in the Strait of Gibraltar using shore-based marine radar images. *J. Phys. Oceanogr.,* **20,** 374–395.

Wesson, J. C., and M. C. Gregg, 1988: Turbulent dissipation in the Strait of Gibraltar and associated mixing. *Small-Scale Turbulence and Mixing in the Ocean,* J. C. J. Nihoul and B. M. Jamart, Eds., Elsivier, 201–222.

——, and ——, 1994: Mixing at Camarinal Sill in the Strait of Gibraltar. *J. Geophys. Res.,* **99** (C5), 9847–9878.

Ziegenbein, J., 1969: Short internal waves in the Strait of Gibraltar. *Deep-Sea Res.,* **16,** 479–498.

——, 1970: Spatial observations of short internal waves in the Strait of Gibraltar. *Deep-Sea Res.,* **17,** 867–875.